Nanoscale

PAPER

View Article Online
View Journal | View Issue

Cite this: *Nanoscale*, 2015, **7**, 9215

Solvent selection causes remarkable shifts of the "Ouzo region" for poly(lactide-*co*-glycolide) nanoparticles prepared by nanoprecipitation†

Moritz Beck-Broichsitter, Julien Nicolas and Patrick Couvreur*

Received 16th March 2015,
Accepted 20th April 2015

DOI: 10.1039/c5nr01695a

www.rsc.org/nanoscale

Polymer nanoparticles (NPs) offer versatile novel biological features of interest for drug delivery applications. "Ouzo diagrams" allowed for a systematic manufacture of specified colloidal formulations by the widely used nanoprecipitation process. Surprisingly, despite the well-documented relevance of the applied organic solvent for nanoprecipitation, its effect on the actual status of the "Ouzo region" was so far not studied. Herein, investigations were undertaken to account for the potential impact of the solvent type on the "Ouzo diagrams" for poly(lactide-*co*-glycolide) (PLGA) and tetrahydrofuran (THF), 1,4-dioxane, acetone and dimethyl sulfoxide (DMSO). The "Ouzo region" shifted considerably to higher polymer fractions upon solvent change (rank order: THF < 1,4-dioxane < acetone < DMSO). Assuming a one-to-one transformation of detached PLGA-bearing solvent droplets (droplet diameter for THF: ~800 nm, 1,4-dioxane: ~700 nm, acetone: ~500 nm and DMSO: ~300 nm) into non-divisible polymer aggregates upon solvent displacement, facilitated to predict the size of NPs found within the "Ouzo region" (size range: 40–200 nm). In conclusion, application of "Ouzo diagrams" is a valuable tool for drug delivery research and will most-likely replace the "trial-and-error"-approach to identify the operating window for the production of stable colloidal formulations by the nanoprecipitation technique.

Introduction

Nanomaterials hold great promise to revolutionize diverse therapeutic approaches currently utilized in medicine.[1–3] For example, drug-loaded nanoparticles (NPs) composed of biocompatible and biodegradable polymers (*e.g.*, poly(lactide-*co*-glycolide) (PLGA)) represent tailored nanocarriers able to selectively accumulate in certain tissues or cells following intravascular administration,[4,5] resulting in an increased therapeutic benefit of the encapsulated medication (*e.g.*, anti-cancer drugs[6,7] and antibiotics[8,9]). In particular, size characteristics greatly affect the pharmacological activity[10] and thus, represent an important design attribute to consider in order to achieve controlled drug release at the desired biological site of action.[11,12]

Nanoparticulate drug delivery vehicles have been prepared from synthetic polymers through various methods including solvent evaporation, salting-out, emulsification-diffusion, and nanoprecipitation; the latter being probably the more easy and popular methodology for NP fabrication.[13–15] Application of the nanoprecipitation process involves the addition of a polymer dissolved in a completely water-miscible organic solvent to an aqueous non-solvent phase, which then instantaneously leads to the formation of submicron particles.[13,16] This convenient one-step manufacturing technique allows the use of less toxic organic solvents (compared to the solvent evaporation process), enables the preparation of polymer NPs without any prior energy input (*i.e.*, emulsification step) and necessitates less tedious purification steps.[13,17,18]

However, a limitation of the nanoprecipitation process is related to the poor control over size characteristics and thus, time-consuming investigations are needed to identify the operating window for the production of specified NPs, owing to the large number of parameters influencing the final product properties.[17,18] In this respect, the introduction of "Ouzo diagrams" – showing the respective amounts of polymer, solvent and non-solvent necessary to obtain stable colloidal formulations – enabled a more systematic manufacture of polymer NPs with defined size characteristics.[19–23] Notably, the impact of solvent nature on the status of the "Ouzo region" was so far rather underestimated.

In this respect, the current study addressed the physicochemical principles associated with polymer NP production by nanoprecipitation, with special emphasis on the solvent type.

Institut Galien Paris-Sud, CNRS UMR 8612, University of Paris-Sud, F-92196, Châtenay-Malabry Cedex, France. E-mail: patrick.couvreur@u-psud.fr; Fax: +33-146835946; Tel: +33-146835396

†Electronic supplementary information (ESI) available. See DOI: 10.1039/c5nr01695a

Depicting a map of compositions, "Ouzo diagrams" for a biodegradable polyester (*i.e.*, PLGA) and four water-miscible organic solvents (*i.e.*, tetrahydrofuran (THF), 1,4-dioxane, acetone and dimethyl sulfoxide (DMSO)) are presented in order to account for potential shifts of the "Ouzo region" upon solvent change. Size characteristics and morphology of the prepared formulations were investigated by dynamic light scattering (DLS) and transmission electron microscopy (TEM). Finally, the experimental results were utilized to predict the size of the polymer NPs found within the individual "Ouzo domains".

Materials & methods

Materials

PLGA, Resomer® RG502H (#1037187; number average molecular weight (M_n): 10.2 kDa, dispersity ($Đ$): 1.8) was acquired from Boehringer Ingelheim (Ingelheim, Germany). Pluronic® F68 (poloxamer 188; M_n: 8.4 kDa, $Đ$: 1.2) was purchased from Sigma-Aldrich (Steinheim, Germany). Filtrated, double-distilled water was obtained from B. Braun (Melsungen, Germany) and used throughout. All other chemicals and solvents were of analytical grade.

Density measurements of polymer solutions

The density of organic PLGA solutions was determined using an oscillating density meter (DMA 4100, Anton Paar, Graz, Austria) at a temperature of 25.0 ± 0.1 °C. Polymer solutions were allowed to equilibrate for 12 h before the measurements.

Preparation and characterization of polymer NPs

PLGA-NPs were prepared by nanoprecipitation at a temperature of 25 ± 1 °C.[21] Briefly, PLGA was dissolved in a water-miscible organic solvent (*i.e.*, THF, 1,4-dioxane, acetone or DMSO) or diverse solvent mixtures (*i.e.*, THF/acetone or DMSO/acetone) for 12 h. The resulting polymer solutions were subsequently injected (injection needle: Fine-Ject® 0.6 × 30 mm; flow rate: 10 mL min^{-1}) into magnetically stirred (500 rpm) water containing 0.1 wt% of poloxamer 188. After injection of the organic phase, the resulting colloidal dispersion was stirred for 10 min under a fume hood and the organic solvent was then removed by rotary evaporation (Rotavapor®, Büchi, Flawil, Switzerland) or dialysis (MWCO: 50 kDa; Spectra/Por® 6, Breda, Netherlands) depending on its boiling point. The actual mass concentration of polymer NPs in the aqueous suspension was determined as previously described.[24] Nanosuspensions were characterized and used directly after preparation.

The hydrodynamic diameter (d_h) and size distribution (PSD) of PLGA-NPs was measured by DLS (non-invasive back scatter technology (λ = 633 nm), scattering angle of 173°) on a Zetasizer NanoZS/ZEN3600 (Malvern Instruments, Herrenberg, Germany). All measurements were performed at a temperature of 25.0 ± 0.1 °C using appropriately diluted samples with at least 10 runs. The optical NP and medium properties (*i.e.*, refractive index and absorption) as well as the dynamic viscosity of the medium were adjusted prior to each measurement.

The morphology of PLGA-NPs was investigated by TEM (JEM-3010 TEM, JEOL, Eching, Germany). Practically, a carbon-coated copper grid (S160-3, Plano, Wetzlar, Germany) was coated with a droplet of dilute nanosuspension and then dried in vacuum.

Proton nuclear magnetic resonance spectroscopic (^{1}H-NMR) experiments (Avance 300, Bruker, Wissembourg, France) were carried out to account for residual solvent in the final nanosuspension. PLGA-NPs were prepared as described above using acetone as solvent and D_2O (Sigma-Aldrich, Steinheim, Germany) containing 0.1 wt% of poloxamer 188 as non-solvent phase. As it can be seen from the ESI (Fig. S1†) the evaporation process was sufficient for complete removal of the organic solvent (no acetone signal at 2.2 ppm[25]).

Solvent-induced swelling of PLGA-NPs (particle size: ~100 nm, final concentration: 1 mg mL^{-1}) was analyzed after incubation of nanosuspension with increasing amounts (0.1–20 wt%) of THF, 1,4-dioxane, acetone and DMSO for 12 h at a temperature of 25 ± 1 °C. Results are expressed as relative particle size changes compared to values obtained for the original nanosuspension. Relevant swelling of PLGA-NPs was only observed with THF and 1,4-dioxane at concentrations ≥10 wt% (ESI, Fig. S2†), in general agreement with results from a previous study.[20] Thus, an artificial change of NP size due to residual solvent in the nanosuspension could be excluded (ESI, Fig. S1 and S2†).

Construction of "Ouzo diagrams"

As a map of compositions a right triangle, three-component phase diagram ("Ouzo diagram"), was chosen and constructed as previously described.[21,26] Therefore, organic polymer solutions were added to the aqueous non-solvent phase to reach the desired final mass fractions in the ternary system. The mass fraction of PLGA (f_{PLGA}) was plotted on the abscissa and the mass fraction of solvent (f_s) could be found on the ordinate (ESI, Fig. S3†). The fraction of the aqueous non-solvent (f_w) was found by the difference ($f_w = 1 - f_{PLGA} - f_s$). The left boundary of the "Ouzo domain" (miscibility-limit curve) became apparent by a sudden increase in intensity of scattered light/turbidity. The right boundary (stability-limit curve) was determined by comparing the absorption (λ = 600 nm; Ultrospec® 3000, Pharmacia Biotech, Freiburg, Germany) of raw and filtered (1.0 μm; Acrodisc®, PALL, Dreieich, Germany) nanosuspensions.[20]

Statistics

All measurements were carried out in triplicate and values are presented as the mean ± standard deviation (SD) unless otherwise noted. Statistical calculations were performed using the software StatGraphics (Statpoint Technologies, Warrenton, USA).

Results & discussion

The nanoprecipitation technique represents a versatile process for the fabrication of colloidal formulations intended for drug delivery purposes.[13–15] NPs can be prepared from numerous synthetic polymers (including biodegradable poly(alkyl cyanoacrylate)[27,28] and polyesters[16,21,29–37]) through this approach. Moreover, diverse matter (including low molecular weight drugs,[21,30,33] fluorescent dyes,[27] high molecular weight drugs like nucleic acids,[33,37] quantum dots[37] and carbon nanotubes[38]) can be encapsulated in the polymer matrix. However, defined size characteristics of these formulations represent a prerequisite to achieve preferential accumulation within the desired target organ.[11,12] For example, to reach tumoral tissues or the bone marrow a particle size of <200 nm and preferentially <100 nm is needed in order to overcome the permeable walls of the vasculature.[39,40]

The molecular mechanisms of instantaneous NP formation by nanoprecipitation involve complex interfacial hydrodynamic phenomena.[14,15] Here, variations of the physicochemical properties along the interface condition mechanical mixing between the two non-equilibrated liquid phases (*interfacial turbulence*), in order to compensate discrepancies in free energy.[13,16,18] Thus, the spontaneous mixing process results in polymer partition into the aqueous non-solvent phase, which then aggregates into colloidal polymer particles upon solvent displacement (*diffusion-stranding* mechanism).[18] Apart from the polymer molecular weight[34,41,42] and the ratio of solvent to non-solvent phase,[29,31–33,36,43] preparation variables, such as the choice of the organic solvent,[17,18,20,21,33,36] and the initial polymer concentration in the organic phase[17,20,21,29,31–36,41–43] were reported to influence the properties of the final NP product. Likewise, the size of polymer NPs (size range: 66–223 nm) prepared in the current study was on one hand a function of the utilized organic solvent (Fig. 1; ESI, Fig. S5A†) and on the other hand a function of the organic polymer concentration (Fig. 1). Although the organic solvent and the initial polymer concentration had a pronounced effect on the size of PLGA-NPs, no relevant change of the particle size distribution was observed (PSD: ~0.05–0.15, which indicates narrowly distributed NP formulations) (ESI, Fig. S4 and S6†).

The extent of solvent diffusion (polymer partition) can be qualitatively described by comparing the individual solvent–water interaction parameters (χ_{s-w})[17,32,36]

$$\chi_{s-w} = V_s/RT(\delta_s - \delta_w)^2 \quad (1)$$

with V_s as the molar volume of the organic solvent, R the universal gas constant, T the absolute temperature, and δ_s and δ_w the total solubility parameters of the solvent and water, respectively. Considering initial organic polymer concentrations between 10 and 25 mg mL^{-1} (Fig. 1), the observed size change of polymer NPs correlated well with the calculated χ_{s-w} (Fig. 2).

Organic solvents displaying a higher water affinity, which is indicated by a lower χ_{s-w} value (*i.e.*, DMSO < acetone < 1,4-dioxane < THF), promoted more efficient solvent diffusion (polymer partition) into the aqueous phase, which in turn conditioned the formation of smaller colloidal formulations.[17,33,36] Application of solvent blends (*i.e.*, THF/acetone and DMSO/acetone) for NP preparation generally supported this finding (ESI, Fig. S5B†).

Furthermore, the size of PLGA-NPs increased for all investigated solvents in an almost linear fashion upon elevation of the polymer concentration in the organic phase (Fig. 1). Accurately, an enhancement from 10 to 25 mg mL^{-1} caused a size

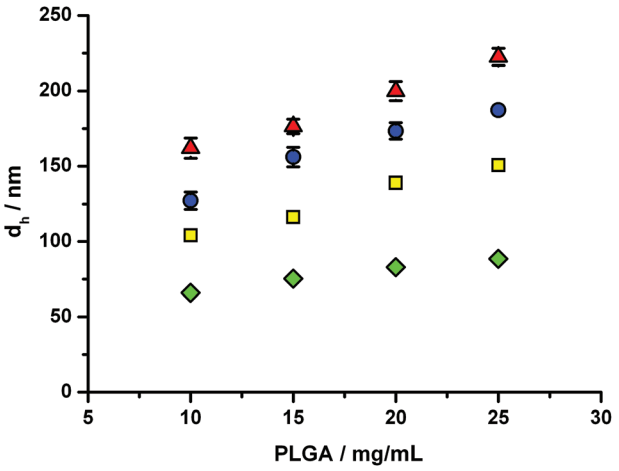

Fig. 1 Size characteristics of PLGA-NPs (d_h) as a function of the initial polymer mass concentration in the organic phase. 1 mL of organic phase (triangles: THF, circles: 1,4-dioxane, squares: acetone, diamonds: DMSO) containing increasing amounts of PLGA was injected into 5 mL of water containing 0.1 wt% of poloxamer 188. Values are presented as the mean ± SD (n = 4). No SD bars are shown if SD fell into the symbol.

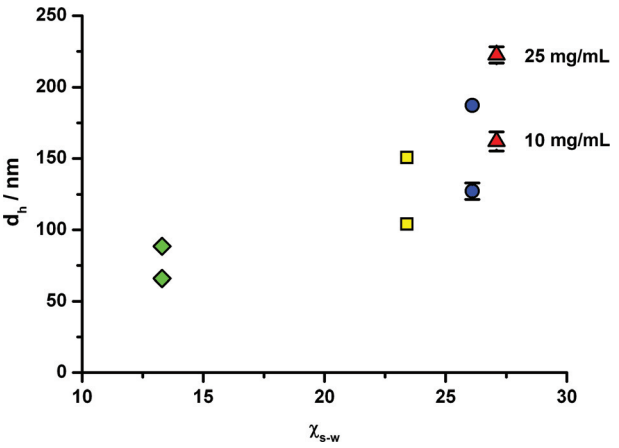

Fig. 2 Influence of the χ_{s-w} on the size characteristics of PLGA-NPs (d_h) for initial organic polymer mass concentrations of 10 and 25 mg mL^{-1} (triangles: THF, circles: 1,4-dioxane, squares: acetone, diamonds: DMSO). Size results were reproduced from Fig. 1 and are presented as mean ± SD (n = 4). No SD bars are shown if SD fell into the symbol.

change from 66 to 89 nm and 162 to 223 nm for DMSO and THF, respectively. In order to further understand the specific nature of the *diffusion-stranding* mechanism responsible for polymer NP formation, the number of PLGA-NPs in aqueous suspension was estimated (Fig. 3A). The number concentration for the four tested organic solvents remained constant despite the increased total polymer amount introduced into the system. However, when comparing the employed solvents, considerable different final PLGA-NP number concentrations (*e.g.*, THF: ~7×10^{11} mL^{-1} and DMSO: ~1×10^{13} mL^{-1}) were obtained.

These findings documented that the addition of the organic polymer solution to the aqueous non-solvent phase resulted in a detachment of uniform polymer-bearing solvent droplets, which then most-likely underwent a one-to-one transformation into polymer NP upon solvent displacement. Thereby, the final size of PLGA-NPs can be directly related to the polymer concentration in the organic phase (*residual core method*)[35] and the relationship between d_h and the droplet size (d_d) can be approximated by

$$d_h = d_d(\rho_d/\rho_p c_{PLGA})^{1/3} \quad (2)$$

with ρ_d and ρ_h as the density of the detaching droplets and the polymer NPs in aqueous suspension[44] and c_{PLGA} as the organic PLGA concentration. Under the current experimental conditions, the calculated droplet size amounted to ~800, ~700, ~500 and ~300 nm for THF, 1,4-dioxane, acetone and DMSO, respectively (Fig. 3B).

In order to further improve the applicability of the nanoprecipitation process for drug delivery, recent studies suggested to replace the above described time-consuming, "trial-and-error"-approach by phase diagrams depicting polymer/solvent/non-solvent fractions necessary to obtain defined colloidal formulations.[19,22] At specified concentrations, the three components fall into the metastable "Ouzo region", where local supersaturation allows for spontaneous polymer precipitation in the form of stable nanosuspensions.[20,21,23] The "Ouzo region" is found between the miscibility-limit and stability-limit curve,[19,22,26] which is in a very narrow range, with respect to the final fraction of polymer.[20,21,23,29] Therefore, only the magnified left part of the triangular phase diagram is presented as a right triangle "Ouzo diagram" using a logarithmic scale for the f_{PLGA} (Fig. 4; ESI, Fig. S7†).

The mixtures represented by the open triangles (left hand) appeared as transparent phases. The onset of the "Ouzo region" (closed symbols) was observed by an abrupt increase in sample turbidity (transition of solutions to nanosuspensions), which always occurred immediately after the combination of the three components. PLGA-NP formulations found within the "Ouzo region" were of homogeneous nature, as confirmed by TEM and DLS analysis (PSD: <0.2) (ESI, Fig. S8†). Further enhancement of f_{PLGA} led to transgression of the "Ouzo region" (open triangles (right hand)), where large polymer particles, aggregates and pellets were formed in addition to NPs (unstable "Ouzo domain"). The "Ouzo region" shifted considerably to higher f_{PLGA} upon change of the organic solvent (rank order: THF < 1,4-dioxane < acetone < DMSO) (Fig. 4; ESI, Fig. S7†). The log–log plot shown in Fig. 5 clearly underlined this observation and illustrated that the final size of PLGA-NPs was only dependent on the excess of polymer to organic solvent introduced into the aqueous non-solvent phase and was not a function of the f_s, as indicated by the collapse of performed experiments on one straight line.

Moreover, the slopes of the resulting regression lines were (close to) 1/3 (*i.e.*, THF: 0.38, 1,4-dioxane: 0.40, acetone: 0.33 and DMSO: 0.33), which indicated that the volume per polymer NP was proportional to the amount of PLGA in the initial feed solution (homogeneous nanoprecipitation process).[20,21]

Notably, the current study detected a consistent upper size limit of ~150–200 nm for polymer NPs found within the individual "Ouzo regions" (Fig. 5). Exceeding the stability-limit curve led to formulations with broader size distribution (PSD:

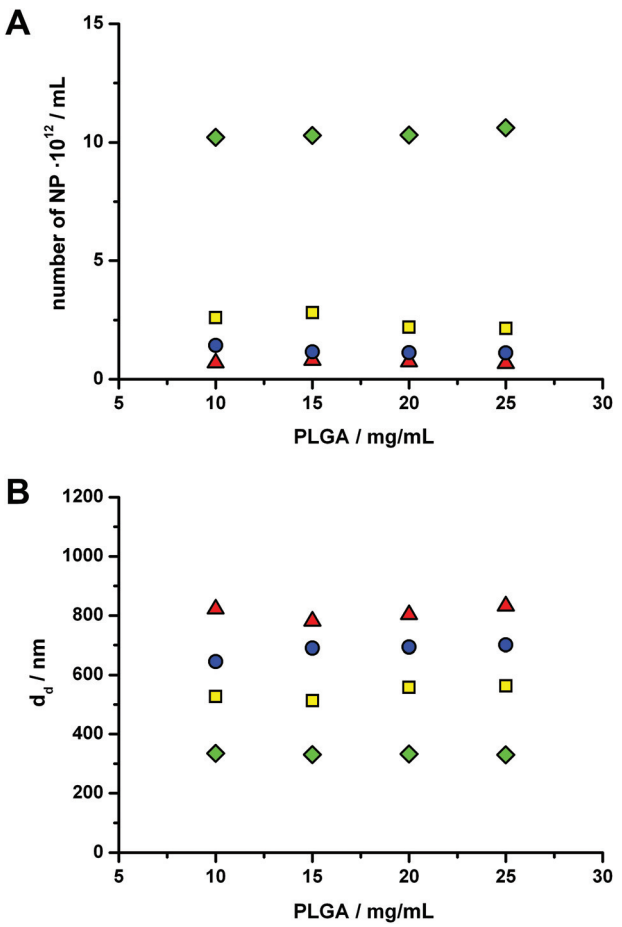

Fig. 3 Estimated number concentrations of PLGA-NPs in aqueous suspension (A) and size of detached polymer-containing solvent droplets (d_d) (B) as a function of the initial PLGA mass concentration in the organic phase (triangles: THF, circles: 1,4-dioxane, squares: acetone, diamonds: DMSO). Calculations were performed with the results found in Fig. 1 and eqn (2).

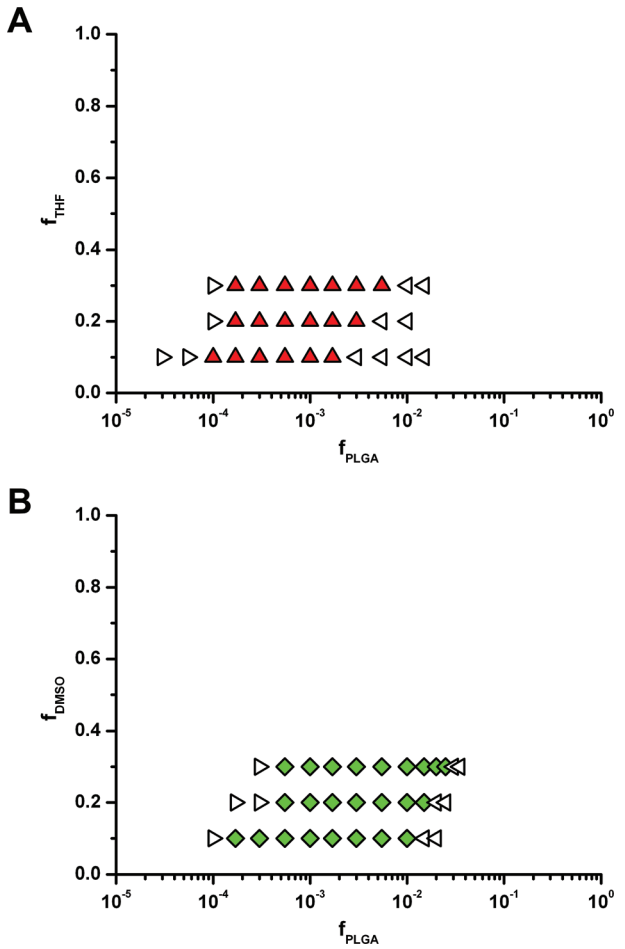

Fig. 4 Experimental "Ouzo diagrams" for ternary systems composed of PLGA, organic solvent ((A) THF and (B) DMSO) and water (containing 0.1 wt% poloxamer of 188) at 25 °C (open triangles (left hand): one phase region, closed symbols: stable "Ouzo region", open triangles (right hand): unstable "Ouzo region").

>0.3) and significant sample flocculation occurred during solvent removal.[20,21,23,29] Zhang *et al.*[42] reported the total interaction energies (*i.e.*, combination of repulsive electrostatic and attractive van der Waals forces) between narrowly and broadly distributed polymer NPs prepared by nanoprecipitation. Accordingly, aggregation of inhomogeneous samples (PSD: >0.3–0.4) is more likely to proceed, due to the low repulsive forces between the approaching, unequal NP. On the contrary, more homogeneous nanosuspensions (PSD: <0.2) reveal higher energy barriers, which prevent aggregation amongst themselves. Hence, the experimentally observed differences in the onset of sample aggregation (Fig. 4 and 5; ESI, Fig. S7†) are attributed to the varying polymer partition capability of the employed organic solvent (Fig. 2). Moreover, it was speculated that further interactions within the polymer/solvent/non-solvent system[20,22,45] or the addition of drugs[21] could influence the actual status of the "Ouzo region".

Finally, knowledge of d_d (Fig. 3) enabled the prediction of the size characteristics of polymer NPs (eqn (2)) found within the operating "Ouzo window". Doing so, the predicted sizes were in excellent agreement with the observed values (Fig. 6; ESI, Fig. S9†).

The slopes of the linear regression lines ($R^2 > 0.98$) ranged between 0.9 (*i.e.*, acetone) and 1.3 (*i.e.*, 1,4-dioxane) for the four applied organic solvents (ESI, Table S1†). Furthermore, the calculated confidence and prediction intervals were found to be very narrow for the current experimental results, what affirmed the quality of the conducted size correlations (ESI, Fig. S9†).

Overall, identification of the underlining mechanisms of the versatile nanoprecipitation process is essential to fabricate nanomedicines with the sizes required for the desired therapeutic application (*e.g.*, personalized medicine)[46] and to prompt their future launching in clinical trials.[3]

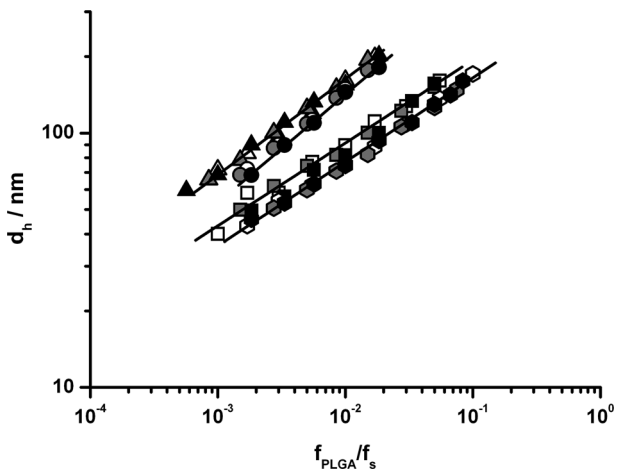

Fig. 5 Log–log plot of the size of PLGA-NPs (d_h) as a function of the excess of f_{PLGA} to f_s (open symbols: f_s = 0.1, gray symbols: f_s = 0.2, closed symbols: f_s = 0.3) for different organic solvent (triangles: THF, circles: 1,4-dioxane, squares: acetone, diamonds: DMSO). The straight lines represent linear fits of the experimental data ($R^2 > 0.98$).

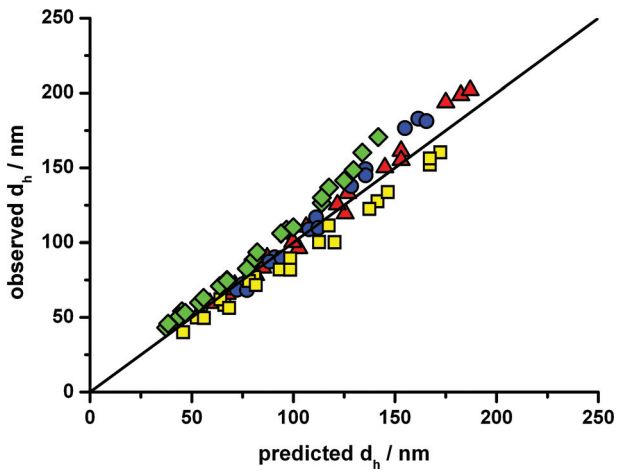

Fig. 6 Correlation of observed and predicted sizes of PLGA-NPs (d_h) found within the "Ouzo region" (triangles: THF, circles: 1,4-dioxane, squares: acetone, diamonds: DMSO). Calculations were performed with the results found in Fig. 3B and eqn (2). The straight line represents a bisectrix of the diagram (slope: 1).

Conclusion

Defining "Ouzo diagrams" for viable polymer/solvent/non-solvent systems represents a meaningful resource for the nanoprecipitation-based synthesis of polymer NPs with specified properties, which is of special interest for drug delivery. Interestingly enough, the "Ouzo region" shifted considerably upon change of the employed organic solvent. This behavior necessitates a substantial adjustment of the PLGA amount to synthesize colloidal formulations with comparable size characteristics. However, preparation of more concentrated nanosuspensions would be useful for numerous therapeutic applications. By elucidating the mechanisms governing the nanoprecipitation process, it became feasible to predict the size characteristics of polymer NPs under the current experimental conditions. These results will assist to further improve the applicability of the nanoprecipitation process for a more systematic construction of promising polymer-based nanomedicines.

Abbreviations

χ_{s-w}	Solvent–water interaction parameter
$Đ$	Dispersity
d_d	Polymer-bearing solvent droplet diameter
d_h	Hydrodynamic diameter of polymer nanoparticles
DLS	Dynamic light scattering
DMSO	Dimethyl sulfoxide
f_{PLGA}	Fraction of poly(lactide-*co*-glycolide)
f_s	Fraction of solvent
f_w	Fraction of water
M_n	Number average molecular weight
MWCO	Molecular weight cut-off
^{1}H-NMR	Proton nuclear magnetic resonance spectroscopy
NPs	Nanoparticles
PLGA	Poly(lactide-*co*-glycolide)
PSD	Size distribution of polymer nanoparticles
R^2	Regression coefficient
SD	Standard deviation
TEM	Transmission electron microscopy
THF	Tetrahydrofuran
wt%	Weight percent

Acknowledgements

MBB is grateful to the "Deutsche Forschungsgemeinschaft" for a personal research scholarship (BE 5308/1-1). This work was further supported by the CNRS and University of Paris-Sud.

References

1 O. C. Farokhzad and R. Langer, *ACS Nano*, 2009, **3**, 16–20.
2 J. Shi, A. R. Votruba, O. C. Farokhzad and R. Langer, *Nano Lett.*, 2010, **10**, 3223–3230.
3 P. Couvreur, *Adv. Drug Deliverty Rev.*, 2013, **65**, 21–23.
4 A. Kumari, S. K. Yadav and S. C. Yadav, *Colloids Surf., B*, 2010, **75**, 1–18.
5 F. Danhier, E. Ansorena, J. M. Silva, R. Coco, A. Le Breton and V. Preat, *J. Controlled Release*, 2012, **161**, 505–522.
6 A. Z. Wang, R. Langer and O. C. Farokhzad, *Annu. Rev. Med.*, 2012, **63**, 185–198.
7 Y. Zhou and J. Kopecek, *J. Drug Targeting*, 2013, **21**, 1–26.
8 N. Abed and P. Couvreur, *Int. J. Antimicrob. Agents*, 2014, **43**, 485–496.
9 X. Zhu, A. F. Radovic-Moreno, J. Wu, R. Langer and J. Shi, *Nano Today*, 2014, **9**, 478–498.
10 W. Jiang, B. Y. Kim, J. T. Rutka and W. C. Chan, *Nat. Nanotechnol.*, 2008, **3**, 145–150.
11 A. Albanese, P. S. Tang and W. C. Chan, *Annu. Rev. Biomed. Eng.*, 2012, **14**, 1–16.
12 S. M. Moghimi, A. C. Hunter and T. L. Andresen, *Annu. Rev. Pharmacol. Toxicol.*, 2012, **52**, 481–503.
13 D. Quintanar-Guerrero, E. Allemann, H. Fessi and E. Doelker, *Drug Dev. Ind. Pharm.*, 1998, **24**, 1113–1128.
14 C. Vauthier and K. Bouchemal, *Pharm. Res.*, 2009, **26**, 1025–1058.
15 J. P. Rao and K. E. Geckeler, *Prog. Polym. Sci.*, 2011, **36**, 887–913.
16 H. Fessi, F. Puisieux, J. P. Devissaguet, N. Ammoury and S. Benita, *Int. J. Pharm.*, 1989, **55**, R1–R4.
17 S. Galindo-Rodriguez, E. Allemann, H. Fessi and E. Doelker, *Pharm. Res.*, 2004, **21**, 1428–1439.
18 C. E. Mora-Huertas, H. Fessi and A. Elaissari, *Adv. Colloid Interface Sci.*, 2011, **163**, 90–122.
19 F. Ganachaud and J. L. Katz, *ChemPhysChem*, 2005, **6**, 209–216.
20 J. Aubry, F. Ganachaud, J. P. Cohen Addad and B. Cabane, *Langmuir*, 2009, **25**, 1970–1979.
21 M. Beck-Broichsitter, E. Rytting, T. Lebhardt, X. Wang and T. Kissel, *Eur. J. Pharm. Sci.*, 2010, **41**, 244–253.
22 E. Lepeltier, C. Bourgaux and P. Couvreur, *Adv. Drug Delivery Rev.*, 2014, **71**, 86–97.
23 X. Yan, M. Delgado, A. Fu, P. Alcouffe, S. G. Gouin, E. Feury, J. L. Katz, F. Ganachaud and J. Bernard, *Angew. Chem., Int. Ed.*, 2014, **53**, 6910–6913.
24 M. Beck-Broichsitter, M. C. Knuedeler, T. Schmehl and W. Seeger, *Pharm. Res.*, 2013, **30**, 16–24.
25 H. E. Gottlieb, V. Kotlyar and A. Nudelman, *J. Org. Chem.*, 1997, **62**, 7512–7515.
26 S. A. Vitale and J. L. Katz, *Langmuir*, 2003, **19**, 4105–4110.
27 B. Le Droumaguet, J. Nicolas, D. Brambilla, S. Mura, A. Maksimenko, L. De Kimpe, E. Salvati, C. Zona, C. Airoldi, M. Canovi, M. Gobbi, M. Noiray, B. La Ferla, F. Nicotra, W. Scheper, O. Flores, M. Masserini, K. Andrieux and P. Couvreur, *ACS Nano*, 2012, **6**, 5866–5879.
28 D. Brambilla, M. Verpillot, B. Le Droumaguet, J. Nicolas, M. Taverna, J. Kóňa, B. Lettiero, H. Hashemi, L. De Kimpe, M. Canovi, M. Gobbi, V. Nicolas, W. Scheper, S. M. Moghimi, I. Tvaroska, P. Couvreur and K. Andrieux, *ACS Nano*, 2012, **6**, 5897–5908.

29 S. Stainmesse, A. M. Orecchioni, E. Nakache, F. Puisieux and H. Fessi, *Colloid Polym. Sci.*, 1995, **273**, 505–511.
30 H. J. Jeon, Y. I. Jeong, M. K. Jang, Y. H. Park and J. W. Nah, *Int. J. Pharm.*, 2000, **207**, 99–108.
31 T. Jung, A. Breitenbach and T. Kissel, *J. Controlled Release*, 2000, **67**, 157–169.
32 U. Bilati, E. Allemann and E. Doelker, *Eur. J. Pharm. Sci.*, 2005, **24**, 67–75.
33 J. Cheng, B. A. Teply, I. Sherifi, J. Sung, G. Luther, F. X. Gu, E. Levy-Nissenbaum, A. F. Radovic-Moreno, R. Langer and O. C. Farokhzad, *Biomaterials*, 2007, **28**, 869–876.
34 P. Legrand, S. Lesieur, A. Bochot, R. Gref, W. Raatjes, G. Barratt and C. Vauthier, *Int. J. Pharm.*, 2007, **344**, 33–43.
35 M. Fraylich, W. Wang, K. Shakesheff, C. Alexander and B. Saunders, *Langmuir*, 2008, **24**, 7761–7768.
36 A. M. de Oliveira, E. Jäger, A. Jäger, P. Stepanek and F. C. Giacomelli, *Colloids Surf., A*, 2013, **436**, 1092–1102.
37 T. Endres, M. Zheng, A. Kilic, A. Turowska, M. Beck-Broichsitter, H. Renz, O. M. Merkel and T. Kissel, *Mol. Pharmaceutics*, 2014, **11**, 1273–1281.
38 P. Lucas, M. Vaysse, J. Aubry, D. Mariot, R. Sonnier and F. Ganachaud, *Soft Matter*, 2011, **7**, 5528–5531.
39 U. Prabhakar, H. Maeda, R. K. Jain, E. M. Sevick-Muraca, W. Zamboni, O. C. Farokhzad, S. T. Barry, A. Gabizon, P. Grodzinski and D. C. Blakey, *Cancer Res.*, 2013, **73**, 2412–2417.
40 A. Swami, M. R. Reagan, P. Basto, Y. Mishima, N. Kamaly, S. Glavey, S. Zhang, M. Moschetta, D. Seevaratnam, Y. Zhang, J. Liu, M. Memarzadeh, J. Wu, S. Manier, J. Shi, N. Bertrand, Z. N. Lu, K. Nagano, R. Baron, A. Sacco, A. M. Roccaro, O. C. Farokhzad and I. M. Ghobrial, *Proc. Natl. Acad. Sci. U. S. A.*, 2014, **111**, 10287–10292.
41 I. Y. Perevyazko, A. Vollrath, C. Pietsch, S. Schubert, G. M. Pavlov and U. S. Schubert, *J. Polym. Sci., Part A: Polym. Chem.*, 2012, **50**, 2906–2913.
42 C. Zhang, V. J. Pansare, R. K. Prud'homme and R. D. Priestly, *Soft Matter*, 2012, **8**, 86–93.
43 I. Y. Perevyazko, J. T. Delaney Jr., A. Vollrath, G. M. Pavlov, S. Schubert and U. S. Schubert, *Soft Matter*, 2011, **7**, 5030–5035.
44 M. Beck-Broichsitter, C. Ruppert, T. Schmehl, A. Guenther, T. Betz, U. Bakowsky, W. Seeger, T. Kissel and T. Gessler, *Nanomedicine*, 2011, **7**, 341–350.
45 P. van de Witte, P. J. DijKstra, J. W. A. van den Berg and J. Feijen, *J. Polym. Sci., Part A: Polym. Phys.*, 1996, **34**, 2553–2568.
46 A. T. Florence and V. H. Lee, *Int. J. Pharm.*, 2011, **415**, 29–33.